Chemistry–A European Journal
Research Article
doi.org/10.1002/chem.202304228
Chemistry Europe
European Chemical Societies Publishing
www.chemeurj.org

Synthesis, Characterization, and Catalytic Application of Colloidal and Supported Manganese Nanoparticles

Johannes Zenner,[a, b] Kelly Tran,[a, b] Liqun Kang,[a] Niklas W. Kinzel,[a, b] Christophe Werlé,[a, c] Serena DeBeer,[a] Alexis Bordet,*[a] and Walter Leitner*[a, b]

Colloidal and supported manganese nanoparticles were synthesized following an organometallic approach and applied in the catalytic transfer hydrogenation (CTH) of aldehydes and ketones. Reaction parameters for the preparation of colloidal nanoparticles (NPs) were optimized to yield small (2–2.5 nm) and well-dispersed NPs. Manganese NPs were further immobilized on an imidazolium-based supported ionic phase (SILP) and characterized to evaluate NP size, metal loading, and oxidation states. Oxidation of the Mn NPs by the support was observed resulting in an average formal oxidation state of +2.5. The MnO_x@SILP material showed promising performance in the CTH of aldehydes and ketones using 2-propanol as a hydrogen donor, outperforming previously reported Mn NPs-based CTH catalysts in terms of metal loading-normalized turnover numbers. Interestingly, MnO_x@SILP were found to lose activity upon air exposure, which correlates with an additional increase in the average oxidation state of Mn as revealed by X-ray absorption spectroscopic studies.

Introduction

Metal nanoparticles (NPs) of first-row transition metals are attracting increasing attention in catalysis, as the availability, cost, and environmental impact of these metals are, in most cases, advantageous compared to widely applied noble metals from the platinum group.[1] In this context, manganese (Mn) would seem a particularly attractive metal as it is the 12th most abundant element and the 3rd most abundant transition metal in the earth's crust.[2] It possesses the lowest global warming potential of all transition metals[3] and most of its typical forms also exhibit low toxicity.[4] In the past decade, organometallic Mn complexes with specifically designed ligands experienced a spectacular development in the field of homogeneous catalysis,[5] with excellent molecular catalysts being reported *inter alia* for (de)hydrogenation[6] and hydrosilylation.[7] In heterogenous catalysis, bulk Mn oxides phases are most commonly used as oxidation catalysts,[8] but also showed activity in hydrogenation of C=C and NO_2 functionalities.[9]

Intriguingly, Mn-based NPs remain largely under-represented in catalysis. This is presumably due to the extreme oxophilicity of Mn, which makes the preparation of size- and composition-controlled NPs difficult.[10] Mn oxide NPs are typically synthesized following bottom-up approaches,[11] such as the thermal decomposition of Mn complexes,[12] permanganate reduction,[13] or sol-gel methods.[12b,14] They find applications in magnetic resonance imaging,[15] biomedical applications,[16] wastewater treatment,[17] and as electrocatalysts for the reduction of oxygen[18] or water oxidation.[8c] Zero- or low-valent Mn NPs received much less attention, and were first reported by Köppler and coworkers *via* the reduction of $MnBr_2$ in tetrahydrofuran (THF), yielding colloidal NPs.[19] Egeberg *et al.* investigated the formation of Mn(0) NPs using pyridine as a solvent, reducing agent for $MnCl_2$, and stabilizer for the resulting NPs.[20] Catalytic applications for low-valent Mn NPs have thus far only been demonstrated by Chakraborty *et al.* They prepared Mn NPs active in the hydrogenation of alkenes and alkynes, formed *in situ* by the reduction of manganese nanoclusters under an atmosphere of H_2.[21]

Overall, studies reporting the preparation, characterization, and application of Mn-based NPs in catalysis are scarce,[22] and often associated with limitations due to high required reaction temperatures,[12b,14] agglomeration[21,23] or degradation[24] under catalytic conditions; as well as low selectivity[14,25] and versatility.[10,20] As a result, the potential of Mn NPs as catalysts has only been tapped upon until now.

Herein, we report a systematic study on the synthesis of colloidal Mn NPs using an organometallic approach, investigating the influence of relevant reaction parameters, as well the chemical nature of potential stabilizing ligand(s). Mn NPs were furthermore immobilized on an imidazolium-based Supported Ionic Liquid Phase (SILP) (Figure 1a). The resulting materials were characterized using various techniques, including electron

[a] J. Zenner, K. Tran, Dr. L. Kang, Dr. N. W. Kinzel, Dr. C. Werlé, Prof. S. DeBeer, Dr. A. Bordet, Prof. W. Leitner
Max Planck Institute for Chemical Energy Conversion
Stiftstr. 34–36, 45470 Mülheim (Germany)
E-mail: alexis.bordet@cec.mpg.de
walter.leitner@cec.mpg.de

[b] J. Zenner, K. Tran, Dr. N. W. Kinzel, Prof. W. Leitner
Institut für Technische und Makromolekulare Chemie
RWTH Aachen University
Worringerweg 2, 52074 Aachen (Germany)

[c] Dr. C. Werlé
Ruhr University Bochum
Universitätsstr. 150, 44801 Bochum (Germany)

Supporting information for this article is available on the WWW under https://doi.org/10.1002/chem.202304228

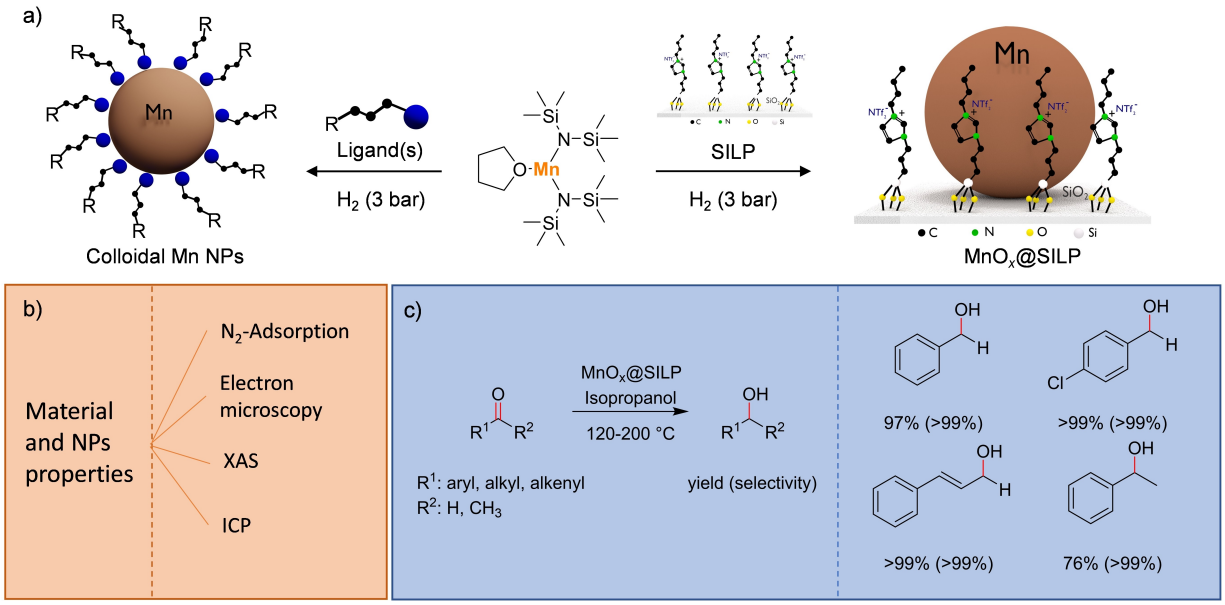

Figure 1. (a) Synthetic pathways for the synthesis of colloidal Mn nanoparticles (NPs) and MnO_x@SILP; (b) characterization methods used to investigate the prepared materials; (c) MnO_x@SILP as a catalyst for the catalytic transfer hydrogenation of aldehydes and ketones.

microscopy and X-ray absorption spectroscopy (XAS) (Figure 1b). The catalytic performance of Mn NPs was probed in the catalytic transfer hydrogenation (CTH) of aldehydes and ketones (Figure 1c), evidencing a crucial influence of the NPs' oxidation state.

Results and Discussion

Synthesis of Colloidal Mn NPs

$[Mn[N(SiMe_3)_2]_2(THF)]$ was synthesized according to a previously reported procedure and used as a precursor for the organometallic synthesis of Mn NPs.[26] This precursor was selected for its high reactivity, allowing reduction under mild conditions, and for the lability of the ligands that can be readily removed from the NPs' surface.[27] In a typical synthesis, $[Mn[N(SiMe_3)_2]_2(THF)]$ was dissolved in dry and degassed mesitylene and reduced under an atmosphere of hydrogen (3 bar) in a Fischer-Porter bottle (Figure 2a). Mesitylene was selected as solvent as it has been successfully employed for the preparation of iron NPs from a precursor of comparable structure, *i.e.* $\{Fe[N(SiMe_3)_2]_2\}_2$.[27–28] The formation and stabilization of colloidal Mn NPs were investigated by varying synthetic parameters such as reaction time, temperature, precursor concentration, and the nature and concentration of stabilizing ligands (Table 1).

Performing the reaction under a standard set of reaction conditions (0.022 $mmol_{[Mn]}$/mL, 150 °C, 3 bar H_2, 18 h) in the absence of additional ligands yielded a dark colloidal solution (Figure 2b) that was stable for several hours under an inert atmosphere (argon), before precipitation started. Interestingly, immediate precipitation of a black material was observed upon exposition of the colloidal solution to air. Transmission electron microscopy (TEM) images of the solution showed mainly large aggregates (Figure 2c), which may have formed due to air exposure during sample preparation. The addition of 1 eq. of PPh_3 to $[Mn[N(SiMe_3)_2]_2(THF)]$ in mesitylene gave a red/brown solution. Upon heating under H_2, the solution quickly turned grey, and precipitation of large particles was observed (Entry 2), indicating that PPh_3 is not a suitable ligand for Mn NPs under

Table 1. Parameter screening in the synthesis of Mn NPs.

Entry	*c* ([**Mn**]) [mmol/mL]	Ligand	Ligand (s): **Mn** (molar ratio)	*T* [°C]	*t* [h]	NP size [nm]
1	0.022	–	0	150	18	aggregates
2	0.022	PPh_3	1:**1**	150	18	aggregates
3	0.022	HDA	1:**1**	150	18	2.2 ± 0.4
4	0.022	PA	1:**1**	150	18	no NPs
5	0.022	HDA: PA	1:1:**1**	150	18	no NPs
6	0.022	HDA: PA	4:3:**2**	150	18	no NPs
7	0.022	HDA	3:**2**	150	18	2.3 ± 0.4
8	0.022	HDA	2:**1**	150	18	2.2 ± 0.4
9	0.022	HDA	3:**1**	150	18	2.4 ± 0.4
10	0.022	HDA	1:**1**	60	18	aggregates
11	0.022	HDA	1:**1**	100	18	aggregates
12	0.022	HDA	1:**1**	175	18	2.3 ± 0.5
13	0.022	HDA	1:**1**	150	6	2.0 ± 0.3
14	0.11	HDA	1:**1**	150	18	2.6 ± 0.5

Conditions: $[Mn[N(SiMe_3)_2]_2(THF)]$ and ligand(s) were dissolved in mesitylene (2 mL) and reduced under an atmosphere of hydrogen (3 bar) in a Fischer-Porter bottle. NP size was determined using transmission electron microscopy (TEM). HDA = hexadecylamine, PA = palmitic acid.

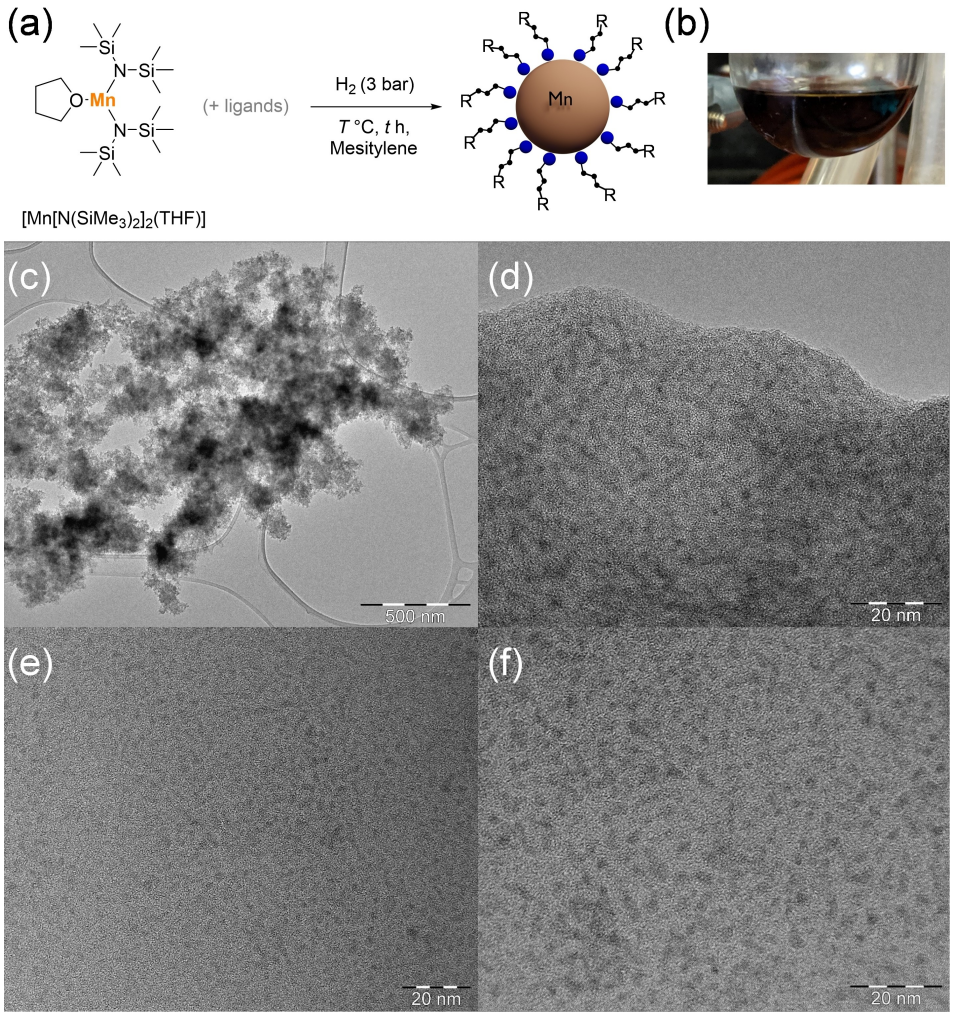

Figure 2. (a) Standard protocol for the synthesis of colloidal Mn NPs and (b) appearance of a resulting solution. Reaction conditions for solution shown in (b): $[Mn[N(SiMe_3)_2]_2(THF)]$ (20 mg, 0.0447 mmol), hexadecylamine (HDA, 1 eq.), mesitylene (2 mL), 150 °C, 18 h. (c)-(f): TEM images Mn NPs prepared according to Table 1. (c) Entry 1: no ligand (Mn aggregates); (d) Entry 3: 1 eq HDA (particle size = 2.2 ± 0.4 nm), (e) Entry 7: 1.5 eq HDA, (particle size = 2.3 ± 0.4 nm) and (f) Entry 14: 1 eq HDA, 5 times higher Mn concentration (particle size = 2.6 ± 0.5 nm). Respective NP size distributions are shown in Figure S2.

these conditions. Using 1 eq. of hexadecylamine (HDA, Entry 3), the resulting black colloidal solution was stable after hydrogenation and could be stored under oxygen-free conditions without precipitation for several months. Even exposure to air did not lead to precipitation in this case. TEM showed the presence of small and well-dispersed NPs (2.2 ± 0.4 nm, Figure 2d).

In contrast, using palmitic acid (PA, Entry 4) yielded a yellow/light orange solution (Figure S1), and no NPs were formed upon hydrogenation. Similar observations were made with mixtures of HDA and PA (Entries 5–6). This is presumably due to the formation of a stable intermediate by reaction between $[Mn[N(SiMe_3)_2]_2(THF)]$ and PA, comparable to the stable Fe carboxylate species observed when mixing $\{Fe[N(SiMe_3)_2]_2\}_2$ with PA.[28]

Increasing the equivalents of HDA did not result in substantial changes in NP size (entries 7–9, Figure 2e, and Figure S3–S4), and small (2–2.5 nm) NPs were obtained in all cases. However, the NPs appeared better dispersed on the TEM grid when more HDA was used (Figure 2e). Reducing the reaction temperature to 100 °C or lower led to partial precipitation of the NPs (entries 10–11, Figure S5). This result can be rationalized by a slower nucleation step leading to fewer nuclei available during the growth process, thus resulting in larger particles. An increase in temperature to 175 °C or a reduction in reaction time from 18 h to 6 h did not significantly impact the resulting NP size (entry 12–13, Figure S6–S7). Based on these results, the reduction of the Mn precursor at 150 °C for 18 h under 3 bar of H_2 with the addition of 1 eq. HDA was selected as the optimized condition. Increasing the Mn and HDA loading by a factor of 5 in the same amount of solvent still yielded small and well-dispersed NPs (Entry 14, Figure 2f).

Mn NPs Immobilized on SILP

The immobilization of metal NPs on support materials is a strategy commonly used to improve their stability and recycla-

bility, in particular for catalytic applications. To demonstrate the possibility of immobilizing Mn NPs prepared following the approach described above, an imidazolium-based ionic liquid phase chemisorbed on silica (SILP) was investigated as a support material. This SILP already proved a suitable matrix for synthesizing and stabilizing various mono- and bimetallic NPs used for hydrogenation and hydrodeoxygenation reactions.[29] In brief, the synthesis of the SILP involved the condensation of [1-butyl-3-(3-triethoxysilylpropyl)-imidazolium] NTf_2 (NTf_2 = bis(trifluoromethanesulfonyl)amide) with dehydroxylated SiO_2.[29a] Mn@SILP (target loading 0.4 $mmol_{Mn}.g_{SILP}^{-1}$) was prepared according to Figure 3a by *in situ* reduction of [Mn[N-($SiMe_3$)$_2$]$_2$(THF)] without additional stabilizer ligand, but in the presence of the SILP under standard conditions (150 °C, 3 bar H_2, 18 h, in mesitylene), yielding a brown powder (Figure 3b). Inductively coupled plasma – optical emission spectroscopy (ICP-OES) measurements revealed a Mn loading of 0.39 $mmol_{Mn}.g_{SILP}^{-1}$ (2.1 wt%), well in agreement with the theoretical value. N_2 adsorption studies of the material (surface area: 266 $m^2.g^{-1}$, pore volume: 0.62 $cm^3.g^{-1}$) showed the expected decrease in BET surface area and pore volume compared to the starting material SiO_2 (surface area: 342 $m^2.g^{-1}$, pore volume 1.07 $cm^3.g^{-1}$)[30] due to the chemisorption of the ionic liquid. Despite a low contrast between Mn and the support material, characterization by scanning transmission electron microscopy in high angle annular dark field mode (STEM-HAADF) evidenced the presence of small and well-dispersed Mn NPs on the SILP (Figure 3c), as confirmed by STEM-HAADF energy dispersive X-ray spectroscopy (EDX) elemental mapping (Figure 3d). However, the low contrast between Mn and the Si-based support made the NPs size determination challenging, and the error on the obtained value of 2.0 nm may be relatively important.

The properties of Mn@SILP were further characterized by XAS. Full details on the data collection, processing, and analysis can be found in the SI (including Table S2-S3, and Figure S9–S12). The Mn K-edge X-ray absorption spectra of Mn@SILP and reference materials (Figure 4a) show that the absorption edge position of Mn@SILP is noticeably higher in energy than that of Mn-foil and MnO, suggesting that oxidized Mn species with an oxidation state higher than +2 dominate the sample. The oxidation of Mn is expected, as previous studies already showed the oxidation of similarly oxophilic Fe NPs by the O-rich SILP support.[29a] Thus, Mn@SILP will from now on be referred to as MnO_x@SILP. Interestingly, a shift of the absorption edge to higher energies and a decrease in the intensity of the white line features can be observed upon exposure of the MnO_x@SILP sample to air (noted MnO_x@SILP_Air in Figure 4), indicating further oxidation of the sample (Figure 4b). The absorption edge position of MnO_x@SILP_Air is shifted to higher energies by approximately 1.0 eV compared to the MnO_x@SILP (Figure S9a). The oxidation states of MnO_x@SILP and MnO_x@SILP_Air can be estimated by comparing the energies of Mn–K edge XAS features to reference materials of different oxidation states in Mn (Figure S11-S12). Using the correlation to the first maximum after the pre-edge feature gives average oxidation states in Mn of +2.6 for MnO_x@SILP and +3.0 for MnO_x@SILP_Air. Correlating the oxidation states to the position of the half-edge jump, the calculated oxidation states are +2.4 and +2.7, respectively.

The EXAFS spectra of MnO_x@SILP and MnO_x@SILP_Air give further information about the coordination structure of the Mn species in the bulk (Figure S9b, S10). Based on the fitting

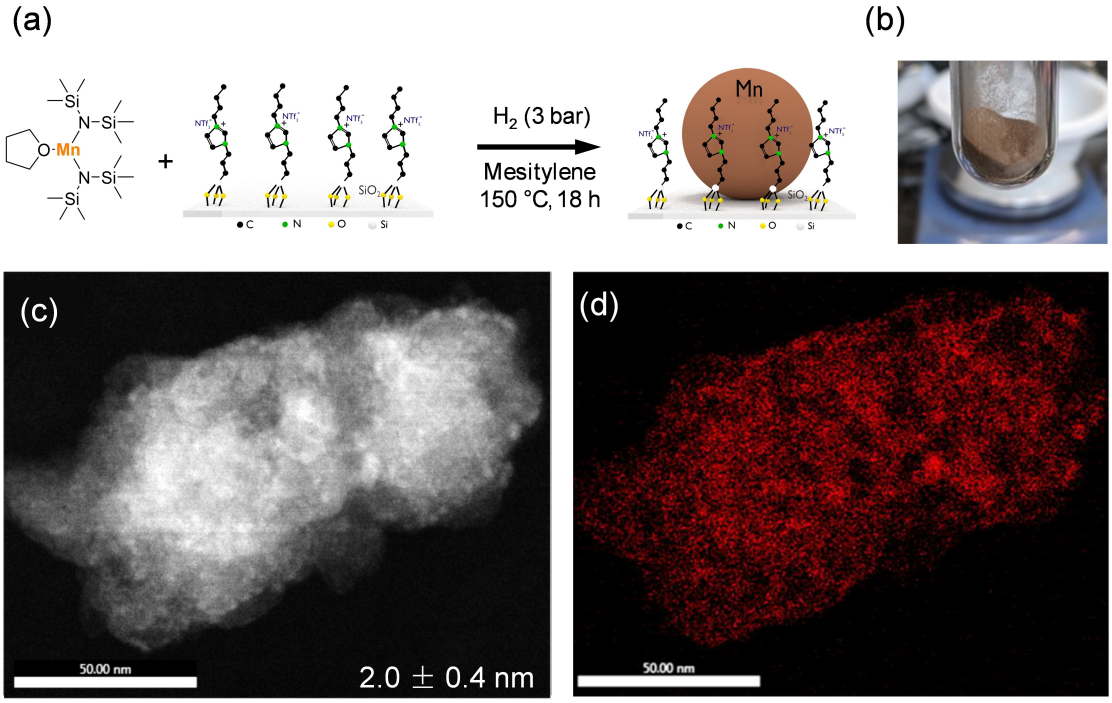

Figure 3. (a) Synthesis and (b) picture of Mn@SILP (for additional images and NP size distribution see Figure S8a–e; (c) STEM-HAADF image of Mn@SILP with (d) STEM-HAADF-EDX elemental mapping of Mn (using Mn Kα fluorescence lines, for EDX spectrum see Figure S8f).

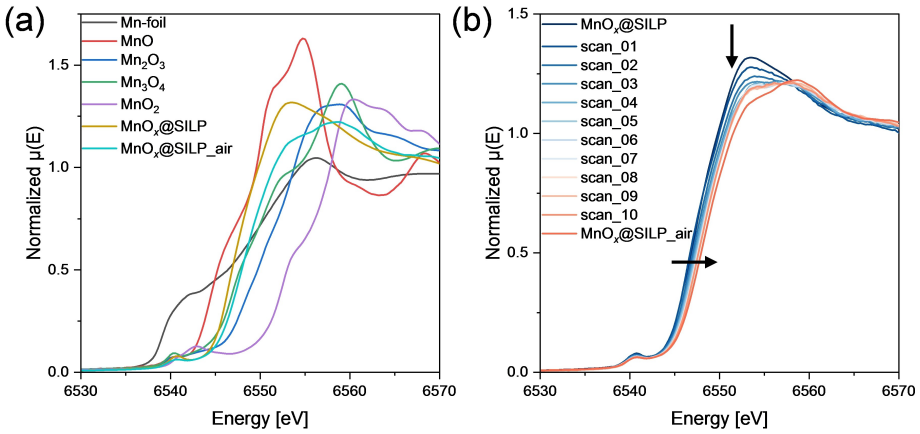

Figure 4. (a) Normalized Mn K-edge XAS spectra of MnO_x@SILP, MnO_x@SILP _Air, and Mn reference materials. (b) In situ Mn K-edge XAS spectra of MnO_x@SILP under oxidizing atmosphere. The first scan (scan_01) was collected after 300 seconds of exposure to air. The interval between the scans is 230 seconds.

results, it is concluded that the Mn species are coordinated by light scatterers (N/O) in the first shell and strongly disordered Mn in the second shell, indicating an amorphous structure. The bond distances do not provide evidence for the presence of metallic Mn–Mn coordination. This is consistent with the Mn K-edge XAS analysis, showing that Mn is present in oxidized form for both MnO_x@SILP and MnO_x@SILP_Air

Catalytic Transfer Hydrogenation of Aldehydes and Ketones Using Mn NPs-based Systems

The catalytic transfer hydrogenation (CTH) of aldehydes and ketones was selected as a model transformation to investigate the performance of the prepared colloidal and supported Mn NPs. In particular, the reduction of benzaldehyde (**1**) to benzyl alcohol (**1a**) using 2-propanol as a solvent and hydrogen donor was studied as prototypical benchmark reaction[12b,31] (Table 2).

Colloidal Mn NPs (synthesized according to the conditions described in Table 1, Entry 14) showed high activity and selectivity toward the formation of **1a** at 170 °C in a closed vessel (97% yield, >99% selectivity, Entry 1). However, significant aggregation and precipitation occurred during the reaction. MnO_x@SILP led to a 98% yield of **1a** under the same reaction conditions (Entry 2). Decreasing the reaction temperature to 150 °C and 120 °C resulted in lower conversions and yields of **1a** (81% and 15%, respectively, Entries 3–4). Analogously prepared $MnO_x@SiO_2$ gave a lower conversion and selectivity than MnO_x@SILP under the same reaction conditions. No conversion was observed with the SILP alone or without catalyst (Entries 6–8).

Despite the rather drastic temperatures, the application of the MnO_x NPs in CTH was found to be quite versatile for a range of carbonyl containing substrates (Table 3, see Table S4 for optimization of reaction conditions). Benzaldehyde derivatives with electron-donating and withdrawing groups (Entries 2–5) in *para*-position were converted to the corresponding alcohols in high yields (75% to >99%) and selectivities (75% to >99%). For 4-methoxybenzaldhyde (Entry 2), the formation of an ether adduct between the substrate and 2-propanol was observed as a side reaction. The CTH of 4-methylbenzaldehyde (Entry 6) consistently yielded a significant amount of an unidentified side product (Figure S13). Satisfyingly, several bio-based aldehydes could also be converted in high yields (71% to >99%) and selectivities (71% to >99%) to the respective alcohols (Entries 7-9). For 5-(hydroxymethyl)furfural (Entry 8), the formation of an ether side product was observed. The CTH of ketones was also successful, even if slightly more challenging than aldehydes, with lower conversions but still high selectivities (Entries 10–12). The CTH of furfuralacetone (Entry 10) yielded small amounts of esterification side products. The conversion of acetophenone could be increased by performing the reaction at 200 °C. However, the selectivity dropped to 30%, with the formation of styrene, (1-isopropoxyethyl)benzene and (oxybis(ethane-1,1-diyl))dibenzene as side products (Table S5).

Table 2. CTH of **1** to **1a** in 2-propanol using various catalysts and conditions.

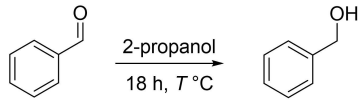

1 **1a**

Entry	Catalyst	T [°C]	X [%]	Y [%]	S [%]
1	Colloidal Mn NPs	170	97	97	>99
2	MnO_x@SILP	170	98	98	>99
3	MnO_x@SILP	150	81	81	>99
4	MnO_x@SILP	120	15	15	>99
5	$MnO_x@SiO_2$	170	64	58	91
6	SILP	170	2	2	>99
7	SILP	150	2	2	>99
8	–	170	0	0	–

Reaction conditions: Mn (0.008 mmol metal) or SILP (20.7 mg), benzaldehyde (22.0 mg, 0.2 mmol, 25 equiv.), 2-propanol (2.0 mL), 18 h, *T* °C, 700 rpm in a 10 mL autoclave; yields were determined by GC-FID using tetradecane as internal standard. *X* = conversion, *Y* = yield, *S* = selectivity

Table 3. CTH of aldehydes and ketones using MnO_x@SILP.

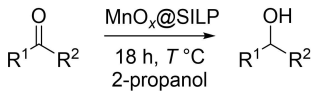

Entry	Substrate	Product	T [°C]	X [%]	Y [%]	S [%]
1			170	98	98	>99
2		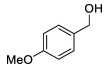	170	>99	75	75
3		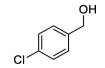	170	>99	>99	>99
4		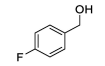	200	>99	>99	>99
5		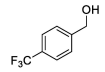	170	98	98	>99
6		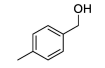	170	85	30	35
7		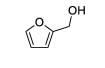	170	87	87	>99
8		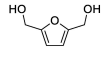	170	>99	71	71
9		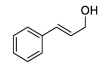	150	>99	>99	>99
10		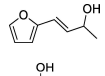	120	60	56	93
11		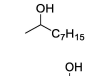	170	60	60	>99
12		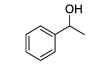	170	74	74	>99

Reaction conditions: Substrate (0.2 mmol, 25 equiv.), MnO_x@SILP (20.7 mg, 0.008 mmol Mn), 18 h, *T* °C, 700 rpm, 2-propanol (2.0 mL); yields were determined by GC-FID using tetradecane as internal standard. *X* = conversion, *Y* = yield, *S* = selectivity.

To get further insight into the reactivity of MnO_x@SILP, a time profile was recorded for the CTH of **1** to **1a** (Figure 5). Results indicate that the reaction follows up to ca 60% conversion a typical first-order kinetic, with an initial reaction rate of $k_{ini} = 0.46\ h^{-1}$. Upon longer reaction time and higher conversion, the rate slows down slightly more than expected from first order kinetics, indicating most likely some catalyst deactivation. Inductively coupled plasma – mass spectrometry (ICP-MS) of the reaction mixture after the CTH of **1** indicated that only 0.01% of Mn leached into the solution, therefore suggesting that Mn leaching is not responsible for catalyst deactivation. Under these conditions, a turnover number (TON) of 24.4 and a turnover frequency (TOF) of $1.4\ h^{-1}$ could be reached, calculated considering the total amount of Mn on the catalyst. These results are substantially higher than those recently reported by Zhou *et al.* (TON = 2.4, TOF = $1.2\ h^{-1}$)[14] and

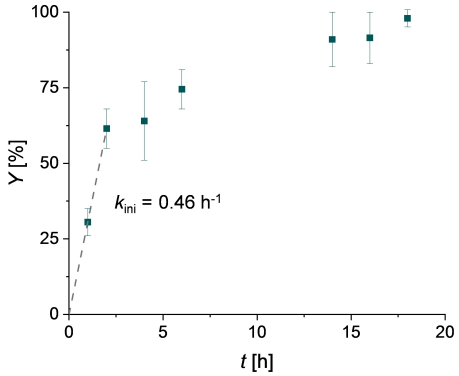

Figure 5. Time profile for the CTH of **1** to **1a** using MnO_x@SILP as a catalyst. Reaction conditions: MnO_x@SILP (20.7 mg, 0.008 mmol Mn), benzaldehyde (22.0 mg, 0.2 mmol, 25 equiv.), 170 °C, t h, 700 rpm, 2-propanol (2.0 mL). Product selectivity to 1a was >99% in all reactions. Yields were determined by GC-FID using tetradecane as an internal standard. Data points are average values of 2 to 3 experiments and error bars represent standard deviations.

Feng *et al.* (TON = 4.0, TOF = $0.3\ h^{-1}$)[12b] using Mn oxide NPs on N-doped carbon supports under similar conditions.

Interestingly, the reactivity of MnO_x@SILP was drastically reduced by a 30 min air exposure before the reaction (Table S5). These results correlate with the important changes in structure and oxidation state observed in the XAS measurements when exposing the sample to air (Figure 4). Therefore, the apparent catalyst deactivation seen in Figure 5 may also be associated with similar changes as the reaction proceeds at high temperature. These results indicate that the catalytic activity of the MnO_x NPs depends critically on their average oxidation state whereby CTH activity is favored at the intermediate oxidation state of +2.5 and lost almost completely upon further oxidation to +3.

CTH reactions using 2-propanol typically follow two main mechanistic pathways.[31b] In Meerwein-Ponndorf-Verley type mechanisms, intermolecular hydride transfer occurs via a six-membered transition state between the metal site, substrate, and hydrogen donor (Figure S14a). In metal-mediated hydrogenations, 2-propanol is dehydrogenated at the metal surface to acetone resulting in hydride species that hydrogenate the substrate (Figure S14b). Using mixture of 2-propanol-d_8 and *tert*-butanol (1:9) resulted in almost exclusive formation of benzyl alcohol with deuterium incorporated in the benzylic position of **1a** as revealed by mass spectrometry and ^1H and ^{13}C NMR analysis (Figure S15–S18). As a much higher degree of H/D-scrambling would be expected for a metal-mediated mechanism,[31b] these data are most consistent with a Meerwein-Ponndorf-Verley type hydride transfer.[12b] Conducting the CTH in pure 2-propanol-d_8 allowed determining the kinetic isotope effect (KIE) of the reaction, with KIE = 3.4 (Figure S19). This primary KIE indicates that the cleavage of the C–H bond in 2-propanol is the rate-determining step.[32]

While the impact of the average oxidation state in small nanoparticles on that mechanism is difficult to rationalize, one might speculate that the higher degree of oxidation results in less vacant Lewis acidic Mn-centers at the surface to accom-

modate the intermolecular hydride transfer between substrate and product.

Conclusions

In conclusion, an organometallic approach using the hydrogenation of $[Mn[N(SiMe_3)_2]_2(THF)]$ as precursor was developed to prepare colloidal as well as supported manganese nanoparticles (Mn NPs) in the 2 nm range with narrow size distribution. The supported nanoparticles show an intermediate oxidation state of slightly above Mn^{2+} after synthesis and are readily oxidized to values close to Mn^{3+} upon exposure to air. The NPs prepared by this method show activity in the Meerwein-Ponndorf-Verley type transfer hydrogenation using 2-propanol as hydrogen donor for a range of carbonyl compounds, with the highest TONs and TOFs reported for Mn NP-based catalysts so far. Interestingly, NPs with the lower oxidation state show higher activity providing new insight for future development of highly active Mn NPs-based catalysts. The presented versatile method for the preparation of highly dispersed and stable colloidal and supported MnO_x NPs is expected to be of interest also for applications in other fields such as magnetic resonance imaging, drug delivery, or electrocatalysis.

Supporting Information

Experimental Section, Supplementary Tables and Figures.

Acknowledgements

The authors acknowledge financial support by the Max Planck Society and by the Deutsche Forschungsgemeinschaft (DFG, German Research Foundation) under Germany's Excellence Strategy – Exzellenzcluster 2186 „The Fuel Science Center" ID: 390919832. L.K. acknowledges the Alexander von Humboldt Foundation for a postdoctoral fellowship and funding support. J.Z. thanks the networking program 'Sustainable Chemical Synthesis 2.0' for support and fruitful discussions across disciplines, and Emanuele Antico for fruitful discussions. We thank Natalia Jakobs and Johanna Taing for N_2(g) adsorption measurements. The authors would like to thank Norbert Pfänder (Max Planck Institute for Chemical Energy Conversion) and Adrian Schlüter (Max-Planck-Institut für Kohlenforschung) for TEM and STEM/EDX analysis. The authors are also thankful to Annika Gurowski, Alina Jakubowski, and Justus Werkmeister (MPI-CEC) for GC and GC-MS measurements. We acknowledge DESY (Hamburg, Germany), a member of the Helmholtz Association HGF, for providing experimental facilities. For parts of this research carried out at PETRA III under proposal I-20211319, we would like to thank Dr. Edmund Welter for assistance in using beamline P65. Diamond Light Source (UK) is acknowledged for experimental time on Beamline B18 under proposal SP31573. We would like to thank Dr. Diego Gianolio, Dr. Iuliia Mikulska, and Dr. Veronica Celorrio for their assistance during the beamtime. Open access funding was provided by Project DEAL. Open Access funding enabled and organized by Projekt DEAL.

Conflict of Interests

The authors declare no conflict of interest.

Data Availability Statement

The data that support the findings of this study are available in the supplementary material of this article.

Keywords: manganese · nanoparticles · catalytic transfer hydrogenation · supported ionic liquid phases · heterogeneous catalysis

[1] a) P. J. Chirik, *Acc. Chem. Res.* **2015**, *48*, 1687–1695; b) I. Roger, M. A. Shipman, M. D. Symes, *Nat. Chem. Rev.* **2017**, *1*, 0003.
[2] *CRC Handbook of Chemistry and Physics*, 103rd edition (Internet Version 2022) ed., CRC Press/Taylor & Francis, Boca Raton, FL, **2022**.
[3] P. Nuss, M. J. Eckelman, *PLoS One* **2014**, *9*, e101298.
[4] M. B. Widegren, M. L. Clarke, *Catal. Sci. Technol.* **2019**, *9*, 6047–6058.
[5] a) M. Garbe, K. Junge, M. Beller, *Eur. J. Org. Chem.* **2017**, *2017*, 4344–4362; b) A. Mukherjee, D. Milstein, *ACS Catal.* **2018**, *8*, 11435–11469; c) P. Schlichter, C. Werlé, *Synthesis* **2021**, *54*, 517–534.
[6] a) S. Elangovan, C. Topf, S. Fischer, H. Jiao, A. Spannenberg, W. Baumann, R. Ludwig, K. Junge, M. Beller, *J. Am. Chem. Soc.* **2016**, *138*, 8809–8814; b) N. A. Espinosa-Jalapa, A. Nerush, L. J. W. Shimon, G. Leitus, L. Avram, Y. Ben-David, D. Milstein, *Chem. Eur. J.* **2017**, *23*, 5934–5938; c) F. Kallmeier, R. Kempe, *Angew. Chem. Int. Ed.* **2018**, *57*, 46–60; d) A. Kaithal, M. Hölscher, W. Leitner, *Angew. Chem. Int. Ed.* **2018**, *57*, 13449–13453.
[7] a) R. J. Trovitch, *Acc. Chem. Res.* **2017**, *50*, 2842–2852; b) L. D. de Almeida, H. Wang, K. Junge, X. Cui, M. Beller, *Angew. Chem. Int. Ed.* **2021**, *60*, 550–565.
[8] a) H. Xu, N. Yan, Z. Qu, W. Liu, J. Mei, W. Huang, S. Zhao, *Environ. Sci. Technol.* **2017**, *51*, 8879–8892; b) L. Miao, J. Wang, P. Zhang, *Appl. Surf. Sci.* **2019**, *466*, 441–453; c) S. Park, Y. H. Lee, S. Choi, H. Seo, M. Y. Lee, M. Balamurugan, K. T. Nam, *Energy Environ. Sci.* **2020**, *13*, 2310–2340.
[9] a) H. G. Manyar, B. Yang, H. Daly, H. Moor, S. McMonagle, Y. Tao, G. D. Yadav, A. Goguet, P. Hu, C. Hardacre, *ChemCatChem* **2013**, *5*, 506–512; b) I. J. McManus, H. Daly, H. G. Manyar, S. F. R. Taylor, J. M. Thompson, C. Hardacre, *Faraday Discuss.* **2016**, *188*, 451–466.
[10] J. F. Bondi, K. D. Oyler, X. Ke, P. Schiffer, R. E. Schaak, *J. Am. Chem. Soc.* **2009**, *131*, 9144–9145.
[11] S. Dawadi, A. Gupta, M. Khatri, B. Budhathoki, G. Lamichhane, N. Parajuli, *Bull. Mater. Sci.* **2020**, *43*, 277.
[12] a) T. D. Schladt, T. Graf, W. Tremel, *Chem. Mater.* **2009**, *21*, 3183–3190; b) Y. Feng, S. Long, G. Yan, B. Chen, J. Sperry, W. Xu, Y. Sun, X. Tang, X. Zeng, L. Lin, *J. Catal.* **2020**, *389*, 157–165.
[13] a) P. Bezdička, T. Grygar, B. Klápště, J. Vondrák, *Electrochim. Acta* **1999**, *45*, 913–920; b) P. Prasad, C. R. Gordijo, A. Z. Abbasi, A. Maeda, A. Ip, A. M. Rauth, R. S. DaCosta, X. Y. Wu, *ACS Nano* **2014**, *8*, 3202–3212.
[14] S. Zhou, G. Chen, X. Feng, M. Wang, T. Song, D. Liu, F. Lu, H. Qi, *Green Chem.* **2018**, *20*, 3593–3603.
[15] T. Kim, E.-J. Cho, Y. Chae, M. Kim, A. Oh, J. Jin, E.-S. Lee, H. Baik, S. Haam, J.-S. Suh, Y.-M. Huh, K. Lee, *Angew. Chem. Int. Ed.* **2011**, *50*, 10589–10593.
[16] a) J. Shin, R. Anisur, M. K. Ko, G. H. Im, J. H. Lee, I. S. Lee, *Angew. Chem. Int. Ed.* **2009**, *48*, 321–324; b) S. Haque, S. Tripathy, C. R. Patra, *Nanoscale* **2021**, *13*, 16405–16426.
[17] a) S. M. Husnain, U. Asim, A. Yaqub, F. Shahzad, N. Abbas, *New J. Chem.* **2020**, *44*, 6096–6120; b) S. Zhu, S.-H. Ho, C. Jin, X. Duan, S. Wang,

Environ. Sci.-Nano **2020**, *7*, 368–396; c) F. He, W. Cai, J. Lin, B. Yu, G. Owens, Z. Chen, *J. Cleaner Prod.* **2021**, *293*, 126207.
[18] a) I. Roche, E. Chaînet, M. Chatenet, J. Vondrák, *J. Phys. Chem. C* **2007**, *111*, 1434–1443; b) M. M. Najafpour, F. Rahimi, E.-M. Aro, C.-H. Lee, S. I. Allakhverdiev, *J. R. Soc. Interface* **2012**, *9*, 2383–2395.
[19] a) R. Franke, J. Rothe, R. Becker, J. Pollmann, J. Hormes, H. Bönnemann, W. Brijoux, R. Köppler, *Adv. Mater.* **1998**, *10*, 126–132; b) J. Sinzig, L. J. de Jongh, H. Bönnemann, W. Brijoux, R. Köppler, *Appl. Organomet. Chem.* **1998**, *12*, 387–391.
[20] A. Egeberg, T. P. Seifert, P. W. Roesky, D. Gerthsen, C. Feldmann, *ACS Omega* **2019**, *4*, 7096–7102.
[21] U. Chakraborty, S. Demeshko, F. Meyer, A. Jacobi von Wangelin, *Angew. Chem. Int. Ed.* **2019**, *58*, 3466–3470.
[22] V. Hoseinpour, N. Ghaemi, *J. Photochem. Photobiol. B* **2018**, *189*, 234–243.
[23] U. Chakraborty, E. Reyes-Rodriguez, S. Demeshko, F. Meyer, A. Jacobi von Wangelin, *Angew. Chem. Int. Ed.* **2018**, *57*, 4970–4975.
[24] F. D. Speck, P. G. Santori, F. Jaouen, S. Cherevko, *J. Phys. Chem. C* **2019**, *123*, 25267–25277.
[25] C. Liu, J.-W. Shi, C. Gao, C. Niu, *Appl. Catal. A* **2016**, *522*, 54–69.
[26] B. Horvath, R. Möseler, E. G. Horvath, *Z. Anorg. Allg. Chem.* **1979**, *450*, 165–177.
[27] F. Dumestre, B. Chaudret, C. Amiens, P. Renaud, P. Fejes, *Science* **2004**, *303*, 821–823.
[28] L.-M. Lacroix, S. Lachaize, A. Falqui, M. Respaud, B. Chaudret, *J. Am. Chem. Soc.* **2009**, *131*, 549–557.
[29] a) K. L. Luska, A. Bordet, S. Tricard, I. Sinev, W. Grünert, B. Chaudret, W. Leitner, *ACS Catal.* **2016**, *6*, 3719–3726; b) A. Bordet, G. Moos, C. Welsh, P. Licence, K. L. Luska, W. Leitner, *ACS Catal.* **2020**, *10*, 13904–13912; c) L. Goclik, L. Offner-Marko, A. Bordet, W. Leitner, *Chem. Commun.* **2020**, *56*, 9509–9512; d) S. Rengshausen, C. Van Stappen, N. Levin, S. Tricard, K. L. Luska, S. DeBeer, B. Chaudret, A. Bordet, W. Leitner, *Small* **2021**, *17*, 2006683; e) S. Sisodiya-Amrute, C. Van Stappen, S. Rengshausen, C. Han, A. Sodreau, C. Weidenthaler, S. Tricard, S. DeBeer, B. Chaudret, A. Bordet, W. Leitner, *J. Catal.* **2022**, *407*, 141–148; f) L. Goclik, H. Walschus, A. Bordet, W. Leitner, *Green Chem.* **2022**, *24*, 2937–2945.
[30] J. Zenner, G. Moos, K. L. Luska, A. Bordet, W. Leitner, *Chimia* **2021**, *75*, 724.
[31] a) M. Chia, J. A. Dumesic, *Chem. Commun.* **2011**, *47*, 12233–12235; b) M. J. Gilkey, P. Panagiotopoulou, A. V. Mironenko, G. R. Jenness, D. G. Vlachos, B. Xu, *ACS Catal.* **2015**, *5*, 3988–3994.
[32] a) P. Nandi, Y. I. Matvieiev, V. I. Boyko, K. A. Durkin, V. I. Kalchenko, A. Katz, *J. Catal.* **2011**, *284*, 42–49; b) T. Komanoya, K. Nakajima, M. Kitano, M. Hara, *J. Phys. Chem. C* **2015**, *119*, 26540–26546.

Manuscript received: December 27, 2023
Accepted manuscript online: February 28, 2024
Version of record online: March 13, 2024